Overview of the Novel Intelligent JAXA Active Rotor Program

Shigeru Saito
Noboru Kobiki
Yasutada Tanabe

Japan Aerospace Exploration Agency
Chofu, Tokyo, Japan

ssaito@chofu.jaxa.jp
kobiki@chofu.jaxa.jp
tan@chofu.jaxa.jp

Wayne Johnson
Gloria K. Yamauchi
Larry A. Young

Aeromechanics Branch
National Aeronautics and Space Administration
Ames Research Center, CA, USA

wayne.johnson@nasa.gov
gloria.k.yamauchi@nasa.gov
larry.a.young@nasa.gov

ABSTRACT

The Novel Intelligent JAXA Active Rotor (NINJA Rotor) program is a cooperative effort between JAXA and NASA, involving a test of a JAXA pressure-instrumented, active-flap rotor in the 40- by 80-Foot Wind Tunnel at Ames Research Center. The objectives of the program are to obtain an experimental database of a rotor with active flaps and blade pressure instrumentation, and to use that data to develop analyses to predict the aerodynamic and aeroacoustic performance of rotors with active flaps. An overview of the program is presented, including a description of the rotor and preliminary pretest calculations.

[1]NOMENCLATURE

A	rotor disk area, πR^2
c	rotor chord
C_T	rotor thrust coefficient, $T/\rho A V_{\text{tip}}^2$
M_{at}	advancing tip Mach number, $M_{\text{tip}}(1+\mu)$
M_{tip}	tip Mach number, V_{tip} divided by speed of sound
N	number of blades
r	blade radial station
R	rotor radius
T	rotor thrust
V	rotor speed
V_{tip}	rotor tip speed
x	blade chordwise coordinate
X/q	rotor drag force divided by dynamic pressure (negative for propulsive force)
z	blade section vertical coordinate
μ	advance ratio, V/V_{tip}
ρ	air density
σ	rotor solidity, $Nc/\pi R$

INTRODUCTION

The capability of active trailing-edge flaps on helicopter rotor blades to reduce vibration (ref. 1) or noise (ref. 2) has been explored in many investigations, with increased interest due to the possibility of actuation by means of smart materials (refs. 3–4). A number of such systems have been tested, including small-scale wind tunnel tests (refs. 5–13), full-scale hover tests (refs. 14–16), full-scale wind tunnel tests (refs. 17–20), and flight tests (refs. 21–22). Development and application of computational fluid dynamics (CFD) methods to the calculation of airloads and noise for rotors utilizing trailing-edge flaps have been progressing (refs. 23–27). Notably absent from all these test campaigns is any measurement of the pressures on the blade and flap. Measured aerodynamic loading is essential for validation of analysis and design tools for rotor blades.

[1] *Presented at Heli Japan 2010, AHS International Meeting on Advanced Rotorcraft Technology and Safety Operations, Ohmiya, Japan, November 1–3, 2010.*

The Japan Aerospace Exploration Agency (JAXA) and the National Aeronautics and Space Administration (NASA) have started the cooperative Novel Intelligent JAXA Active Rotor (NINJA) program. The objectives of the program are to obtain an experimental database of a rotor with active flaps and blade pressure instrumentation, and to use that data to develop analyses to predict the aerodynamic and aeroacoustic performance of rotors with active flaps. The program includes a test of a JAXA pressure-instrumented, active-flap rotor in the National full-Scale Aerodynamics Complex (NFAC) 40- by 80-Foot Wind Tunnel at Ames Research Center.

This paper describes the research program and the rotor design, and presents some results of preliminary pretest calculations.

JAXA/NASA PROGRAM

The overall schedule of the JAXA/NASA Co-operative Research on Helicopter Active Control Technologies is shown in figure 1. JAXA has been engaged in the design of the Novel Intelligent JAXA Active Rotor (NINJA Rotor) for some years, including non-rotating wind tunnel tests (refs. 28–29). In February 2009, JAXA and NASA signed an Agreement "to allow for the testing of JAXA's full-scale rotor with active flap in the National Full-Scale Aerodynamics Complex (NFAC) 40- by 80-Foot Wind Tunnel at Ames Research Center." The NASA team comprises NASA and U.S. Army personnel, at Ames, Langley, and Glenn Research Centers. The JAXA team comprises researchers from the JAXA Aviation Program Group and Aerospace Research and Development Directorate, and Kawasaki Heavy Industries. The program milestones are a whirl tower test of the rotor at Kawasaki in 2013, and the wind tunnel test in the NFAC in 2015. The cooperative program includes extensive calculations of airloads and noise with high-fidelity tools, including pretest predictions and correlation with the wind tunnel data.

PHASE		Phase I Blind Calculation/Comparison			PHASE II				
YEAR		2009	2010	2011	2012	2013	2014	2015	2016
Calculations									
JAXA	Basic Properties Derivation	→							
J/N	Blind Calculation/Comparison with JAXA Blade	→		→					
J/N	Review of Cooperation			▼					
Testing									
JAXA	Manufacture	→		→					
JAXA	Whirl Tower Test				→				
NASA	40x80 Wind Tunnel Test						→		

J=JAXA, N=NASA

Figure 1. JAXA/NASA Co-operative Research on Helicopter Active Control Technologies.

ROTOR DESCRIPTION

The NINJA Rotor has four articulated blades, with a radius of 5.8 m and a nominal chord of 0.4 m. The baseline tip speed is 200 m/sec. Figure 2 shows the blade planform. The AT2 tip shape and AK airfoil contours are based on ATIC research (ref. 28). Table 1 gives the rotor parameters. The hinge offset is 5.7%R.

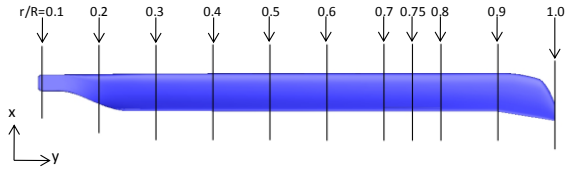

Figure 2. NINJA Rotor blade planform.

Table 1. NINJA Rotor parameters.

radius, R	5.8	m
chord, c	0.4	m
number of blades	4	
flap and lag hinge offset	330	mm
solidity, $\sigma = Nc / \pi R$	0.0878	
torque offset	18	mm
pitch link radial station	330	mm
pitch link offset (forward of pitch axis)	180	mm
nominal twist	–10	deg
pitch link stiffness	TBD	
lag damper	TBD	
flap and lag hinge spring	55000	N-mm/deg
pitch bearing spring	15000	N-mm/deg
Lock number	4.9	
trailing edge flap		
radial extent	70-80	%R
edge gap	2	mm
chord	10	%c
hinge (no gap)	90	%c
airfoils		
$r = 0$ to 80%R	AK120G	
$r =$ tip	AK100G	

Figure 3 illustrates the full-scale onboard active flap system design, which was sized based on the results of ref. 28. The flap span is 10%R and the flap chord is 10%c. Two piezo actuators operate in an out-of-phase reciprocated mode in the directions of

compression and extension. The displacements of the actuators are augmented by an integrated one-piece amplifying mechanism that generates linear reciprocating movement and transmits this driving force to a push-pull linkage by an elastic hinge. The geometrical amplifying index, which is the ratio between the displacement of the tip of the amplifying mechanism and that of actuator, is 10. Finally, the active flap is driven by the linkage through a composite hinge installed between the trailing edge of the blade and the leading edge of the flap. These design features are adopted to suppress free play in the drive mechanism to obtain the target amplitude by the least actuation power.

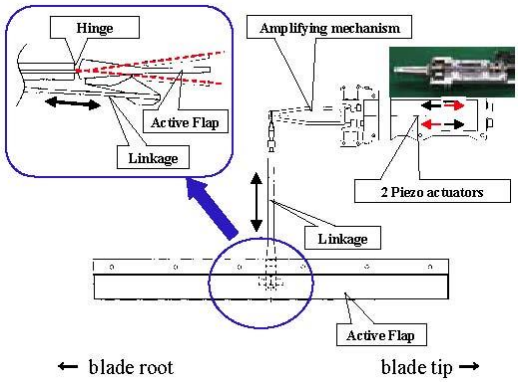

(a) Schematic of active flap system.

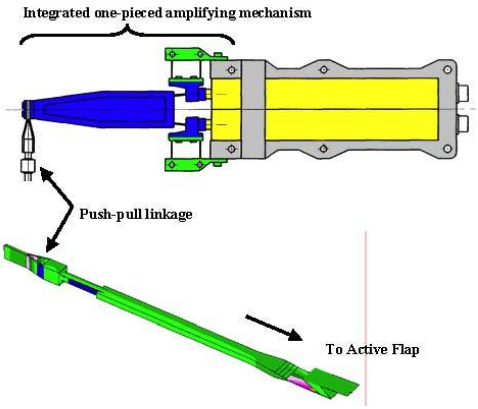

(b) Integrated one-piece amplifying mechanism and push-pull linkage.

Figure 3. Full-scale onboard active flap system (continued)..

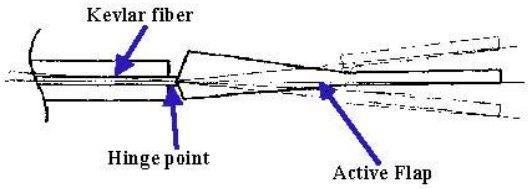

(c) Hinge portion of active flap.

Figure 3. Full-scale onboard active flap system (concluded).

Figure 4 shows the blade chord, twist, and quarter-chord offset from the pitch axis. Figure 5 shows cross-sections of the blade at several radial stations. The blade structural dynamic properties are plotted in figure 6.

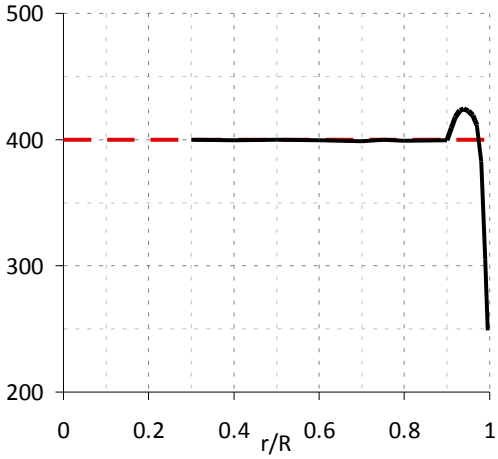

(a) Chord (mm).

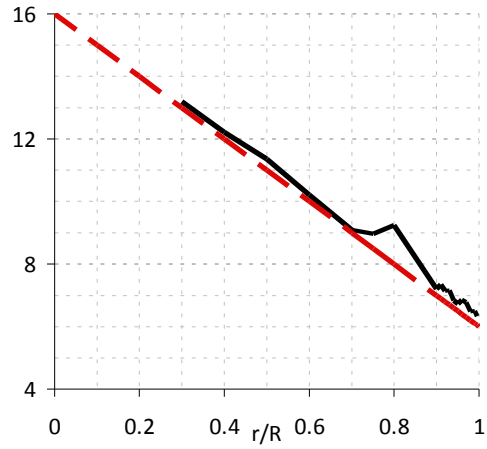

(b) Twist (deg).

Figure 4. NINJA Rotor blade geometry (continued).

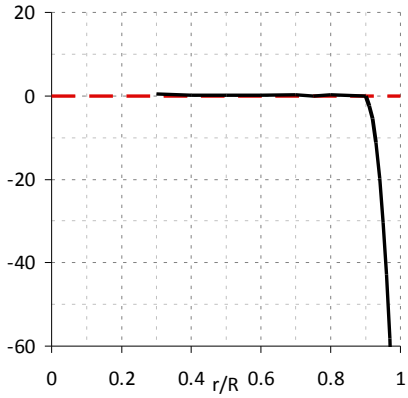

(c) Quarter-chord offset, forward pitch axis (mm).

Figure 4. NINJA Rotor blade geometry (concluded).

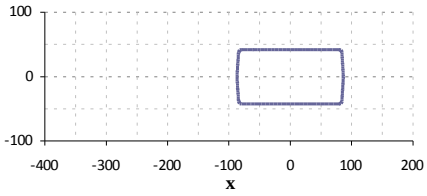

(a) r = 10%R.

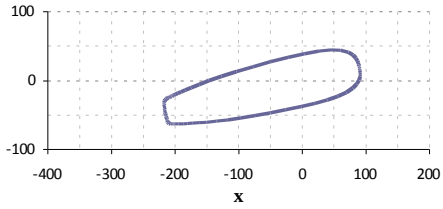

(b) r = 20%R.

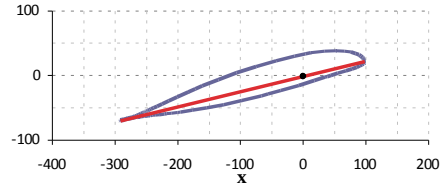

(c) r = 30%R.

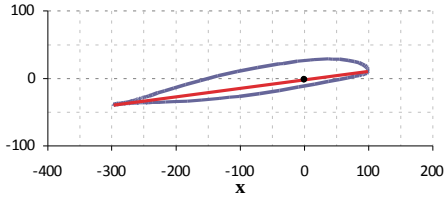

(d) r = 90%R.

Figure 5. NINJA Rotor blade cross-sections (continued).

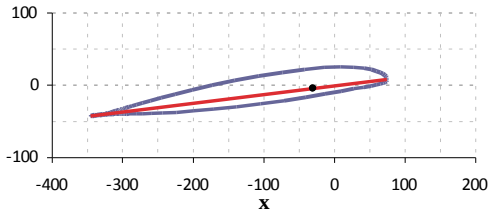

(e) r = 95%R.

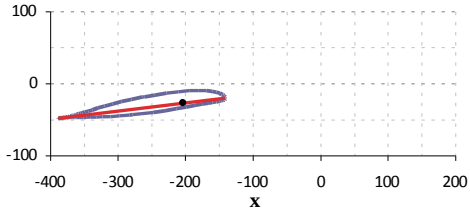

(f) r = 99.5%R.

Figure 5. NINJA Rotor blade cross-sections (concluded).

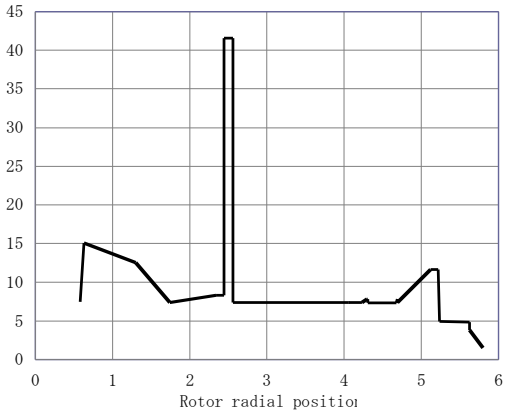

(a) Mass distribution (kg/m).

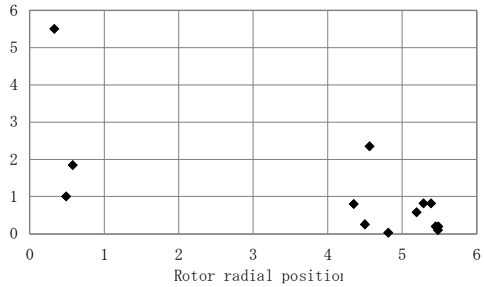

(b) Concentrated mass (kg).

Figure 6. NINJA Rotor blade structural dynamic properties (continued).

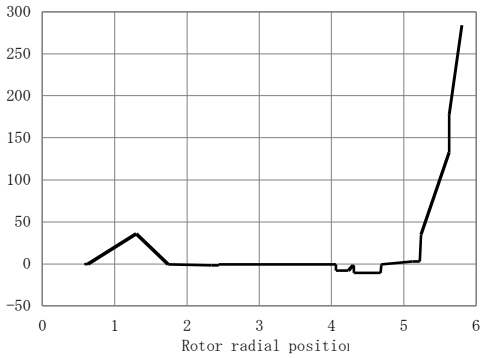

(c) Chordwise CG position, aft of pitch axis (mm).

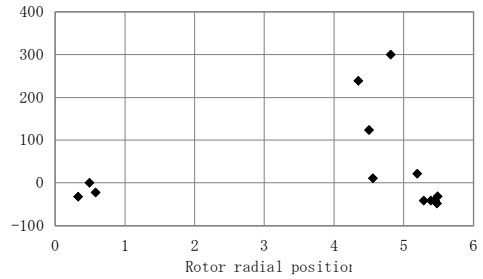

(d) Concentrated mass CG position, aft of pitch axis (mm).

(e) Flapwise moment of inertia (kg-m^2/m).

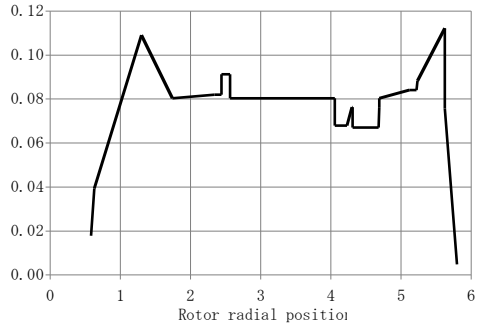

(f) Chordwise moment of inertia (kg-m^2/m).

Figure 6. NINJA Rotor blade structural dynamic properties (continued).

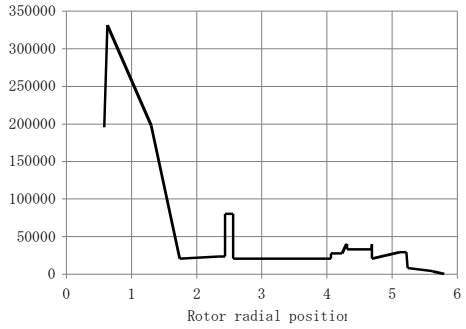

(g) Flapwise bending stiffness (N-m^2).

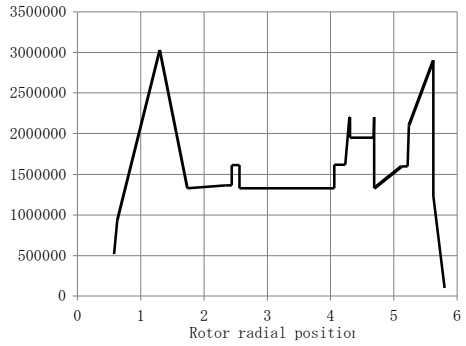

(h) Chordwise bending stiffness (N-m^2).

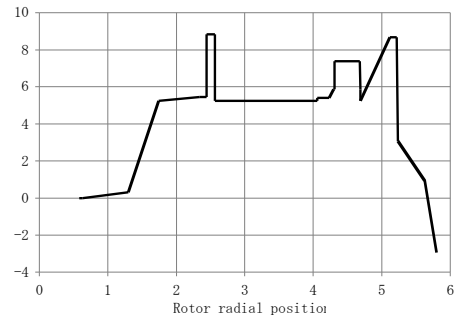

(i) Flapwise neutral axis, above pitch axis (mm).

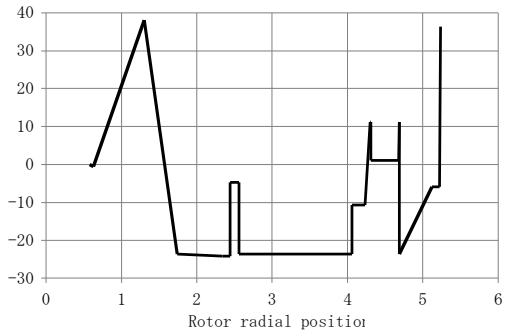

(j) Chordwise neutral axis, aft of pitch axis (mm).

Figure 6. NINJA Rotor blade structural dynamic properties (continued).

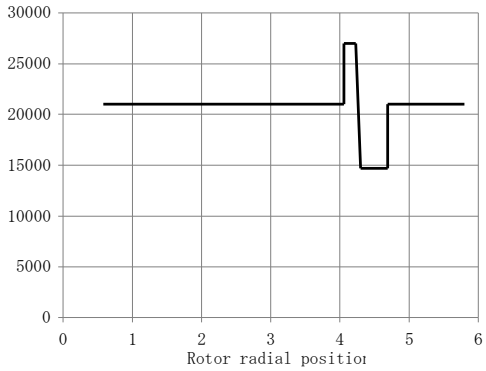

(k) Torsion stiffness (N-m^2).

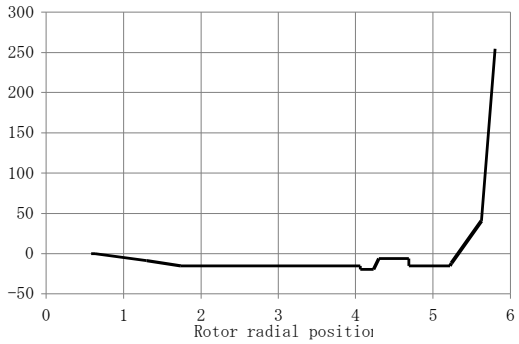

(l) Shear center, aft of pitch axis (mm).

Figure 6. NINJA Rotor blade structural dynamic properties (concluded).

ROTOR INSTRUMENTATION

Two opposing blades will be instrumented for structural load measurements, and two opposing blades will be instrumented for pressure measurements. Table 2 summarizes the two sets of instrumentation. Table 3 lists the radial stations for the structural load instrumentation. Table 4 lists the radial stations and chordwise positions for the pressure instrumentation.

Table 2. Summary of blade instrumentation.

Load Measurement Blades
dynamic loads (14)
active flap deflection at flap midspan
Pressure Measurement Blades
unsteady pressures (31)
active flap deflection at flap edges and midspan
All Blades
pitch link load
active flap hinge moment
actuator displacement (2)
displacement amplifier
actuator input voltage (2)

Table 3. Blade dynamic load instrumentation.

r/R	0.30	0.40	0.50	0.60	0.70	0.85
flap	X	X	X	X	X	X
lead-lag	X		X		X	
torsion	X	X	X	X	X	

Table 4. Blade pressure instrumentation.

r/R	0.65 (2)		0.73 (18)		0.83 (2)		0.90 (9)	
x/c	U (1)	L (1)	U (12)	L (6)	U (1)	L (1)	U (6)	L (3)
0.000			X				X	
0.040	X	X	X	X	X	X	X	X
0.080			X					
0.100				X				X
0.140			X					
0.200			X	X			X	X
0.275								
0.350			X				X	
0.425								
0.500			X					
0.600			X				X	
0.650				X				
0.700			X					
0.800			X	X			X	
0.920			X	X				
0.950								
1.000			X					

WIND TUNNEL INSTALLATION

The 40- by 80-Foot Wind Tunnel has a closed test section with semicircular sides and a closed-circuit air return passage. The test section is lined with sound-absorbing material to reduce acoustic reflections. The test section is 39-feet high, 79-feet wide, and 80-feet long. The maximum test section velocity is approximately 300 knots. The tunnel is managed and operated by the U.S. Air Force Arnold Engineering Development Center (AEDC).

The NINJA Rotor will be installed on the Rotor Test Apparatus (RTA), which is a drive and support system enclosed in a generic fuselage shape. The

RTA can accommodate a variety of rotor diameters and tip speeds. The RTA houses two tandem-mounted, variable speed electric drive motors that can provide up to 3000 horsepower at a maximum of 437 RPM. A 5-component balance mounted on the RTA measures rotor loads at the hub moment center. The balance was designed and fabricated to measure both the steady and vibratory rotor normal, axial and side forces, together with rotor pitch and roll moments up to rotor thrust levels of 22,000 lbs. The balance shares a common centerline with the rotor shaft. An instrumented flex-coupling measures rotor torque and residual normal force. The RTA is mounted on a 3-strut system. The vertical adjustment of the tail strut enables the rotor shaft angle to be varied. Figure 7 shows views of the NINJA Rotor installed on the RTA in the 40- by 80-Foot Wind Tunnel. An acoustic traverse with microphones will be located on the advancing side of the rotor.

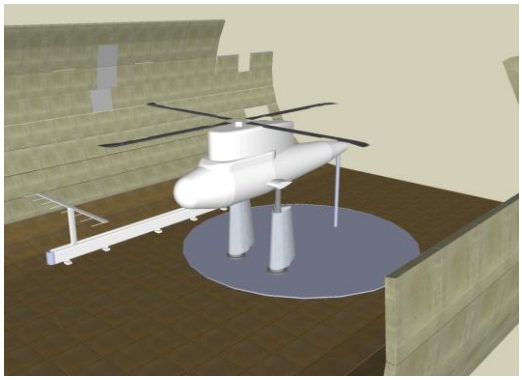

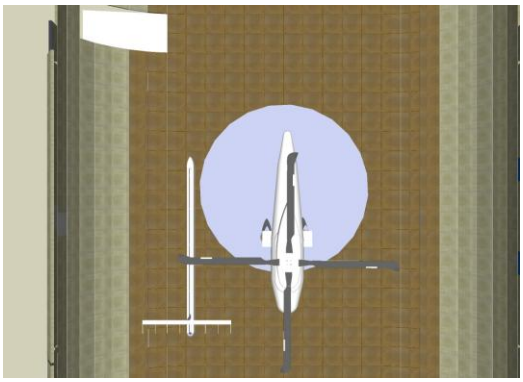

Figure 7. NINJA Rotor installed on the RTA in the 40- by 80-Foot Wind Tunnel (continued).

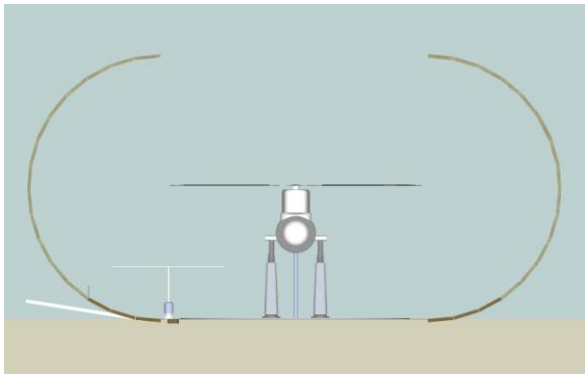

Figure 7. NINJA Rotor installed on the RTA in the 40- by 80-Foot Wind Tunnel (concluded).

PRETEST CALCULATIONS

Analysis Conditions

Table 5 summarizes the key operating conditions identified for pretest calculations: low speed conditions characterized by blade-vortex interaction (BVI), and high-speed conditions characterized by high-speed impulsive noise (HSI).

Table 5. Operating conditions for pretest analysis.

condition		BVI	BVI	HSI	VNE
tip speed	m/s	200	200	200	200
M_{tip}		0.588	0.588	0.588	0.588
thrust	N	35k	35k	35k	35k
C_T		0.0068	0.0068	0.0068	0.0068
C_T/σ		0.0770	0.0770	0.0770	0.0770
V	m/s	30	34	60	78
V	knots	58	66	117	152
μ		0.15	0.17	0.30	0.39
M_{at}		0.68	0.69	0.77	0.82

Comprehensive Analysis

The comprehensive analysis CAMRAD II (ref. 30) was used to calculate the rotor performance, blade loads, and hub loads for a range of operating conditions and active flap motion. The performance calculations are required to help establish the expected power and balance load for the rotor installed on the wind tunnel test module. For example, figure 8 shows the power required as a function of advance ratio, for the baseline thrust

$C_T/\sigma = 0.077$ and a rotor propulsive force of $X/q = -1$ m^2; or constant shaft angle +5 deg (aft); or constant shaft angle –5 deg (forward).

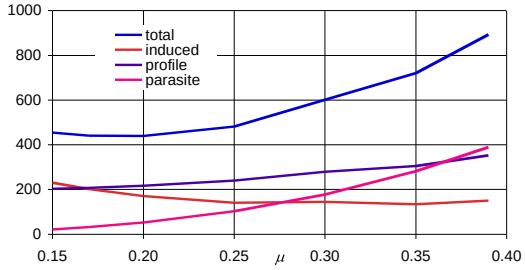

(a) Propulsive force $X/q = -1$ m^2.

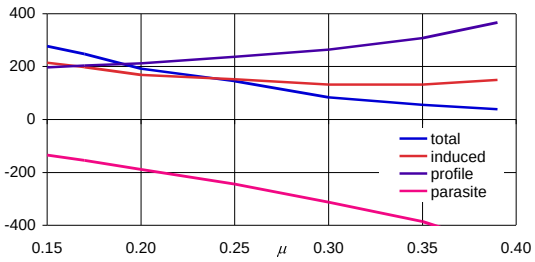

(b) Shaft angle +5 deg (aft).

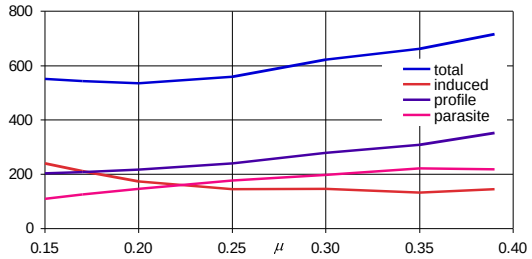

(c) Shaft angle –5 deg (forward).

Figure 8. Calculated forward flight power required, for $C_T/\sigma = 0.077$.

The effectiveness of the active flap to control the rotor behavior was examined by calculations for a flap amplitude of 4 deg, at 2/rev, 3/rev, 4/rev, and 5/rev. The flap phase was swept from 0 to 360 deg. Figure 9 shows the calculated hub loads, control loads, and blade pitch motion as a function of flap input phase, for a BVI condition of $C_T/\sigma = 0.077$, $\mu = 0.17$, and shaft angle –5 deg (aft). Figure 10 shows the calculated loads and motion for an HSI condition of $C_T/\sigma = 0.077$, $\mu = 0.39$, and propulsive force of $X/q = -1$ m^2. The oscillatory hub force magnitude (N) shown is the 4/rev drag, side, and vertical force in shaft axes. The pitch link load shown is the one-half peak-to-peak value. The harmonics of the blade root pitch and tip pitch motion in response to the 3/rev active flap input are shown. For the pitch link stiffness used, there is substantially more elastic twist than elastic root pitch deflection. At high speed, the 3/rev active flap input results in some 2/rev and 4/rev blade torsion motion.

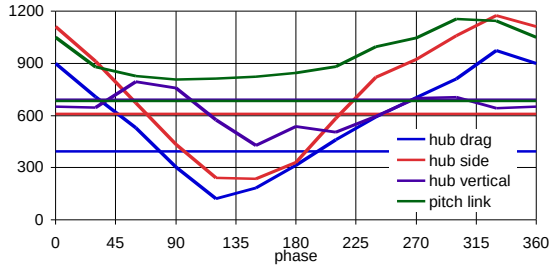

(a) Oscillatory hub force magnitude (4/rev) and one-half peak-to-peak pitch link load.

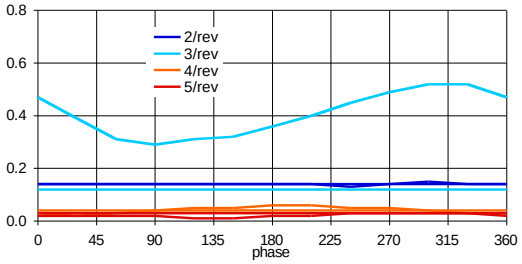

(b) Harmonics of root pitch magnitude.

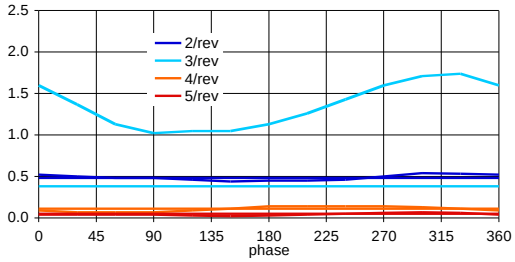

(c) Harmonics of tip pitch magnitude.

Figure 9. Calculated hub loads (N), control loads (N), and blade pitch motion (deg) as a function of flap input phase; 4 deg 3/rev flap motion; for BVI condition ($\mu = 0.17$, shaft angle = 5 deg aft).

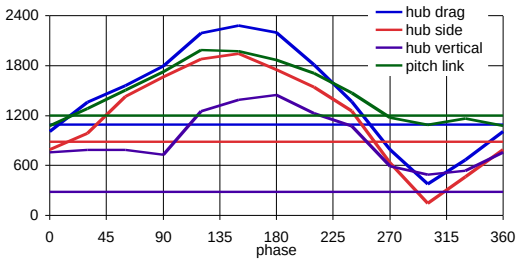

(a) Oscillatory hub force magnitude (4/rev) and one-half peak-to-peak pitch link load

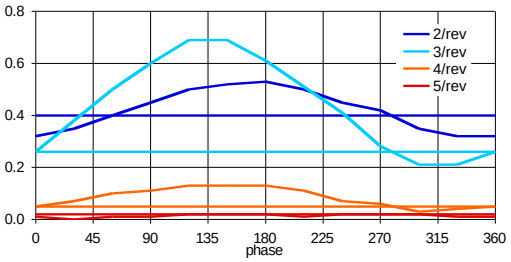

(b) Harmonics of root pitch magnitude

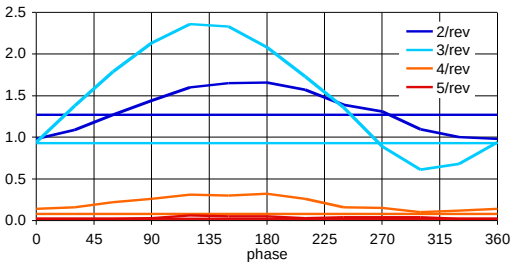

(c) Harmonics of tip pitch magnitude

Figure 10. Calculated hub loads (N), control loads (N), and blade pitch motion (deg) as a function of flap input phase; 4 deg 3/rev flap motion; for HSI condition ($\mu = 0.39$, $X/q = -1$ m^2.).

Figure 11 shows the calculated in-vacuum blade frequencies as a function of rotor speed. The results are based on an estimated pitch link stiffness of 500,000 N/m. The actual stiffness must be obtained by measurement on the whirl stand and the wind tunnel test module. Figure 11 shows calculations by JAXA and NASA.

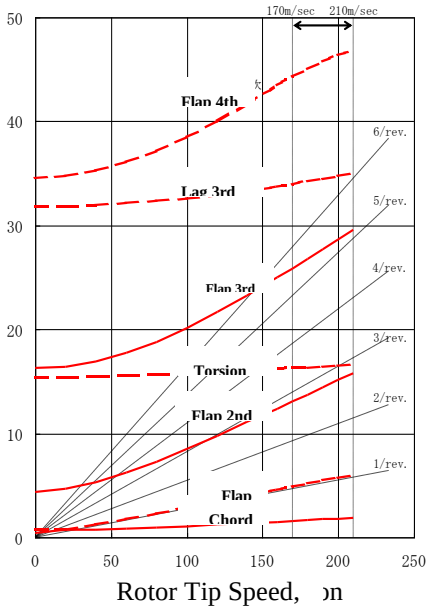

a) JAXA calculation

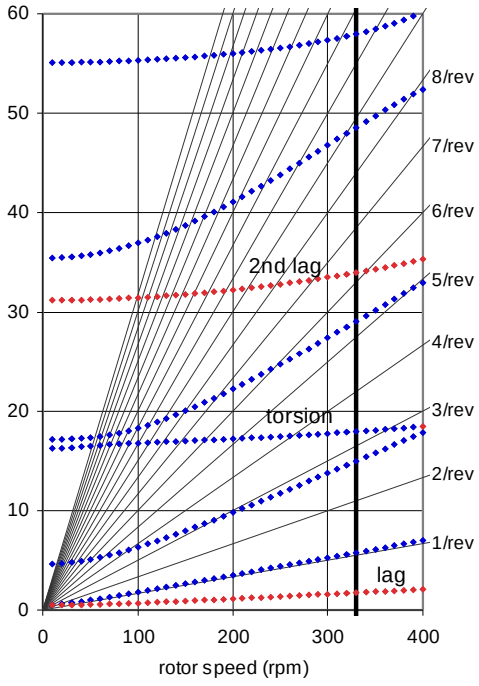

(b) NASA calculation

Figure 11. NINJA Rotor calculated in-vacuum blade frequencies (pitch link stiffness = 500,000 N/m).

Aerodynamic Predictions

The aerodynamic performance has been conducted in hovering flight conditions by using the rFlow3D code developed by JAXA. Figure 12 shows the grid system in this calculation. The coarse grid is used.

The calculation region extends out to 20R in the x- and y-directions and out to 8R in the z-direction. The number of grid points is approximately 8.5 million. This number of grid points is not sufficient for BVI capturing but should be sufficient for aerodynamic performance.

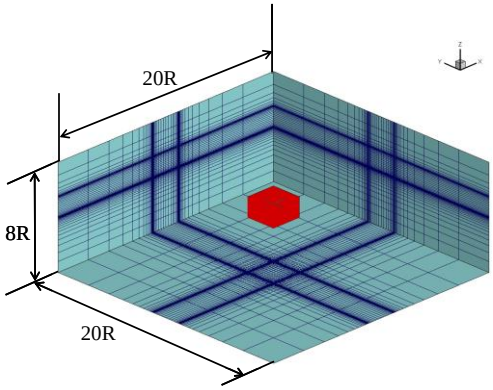

(a) Grid

Inner back Grid	232 × 232 × 145 (X × Y × Z)
Outer back Grid	101 × 101 × 101 (X × Y × Z)
Blade Grid	141 × 101 × 15 (span× chord × normal)
Spacing of Inner back grid size	0.15c (Coarse grid)

(b) Grid point distribution

Figure 12. Grid system in rFlow3d.

The aerodynamic performance in hover was calculated. Figure 13 shows the rotor thrust and torque versus blade pitch angle. In this calculation, an Euler formulation is used, so the torque is under-predicted because of the lack of skin friction.

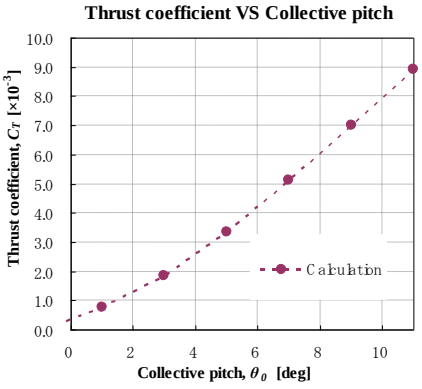

(a) Thrust coefficient vs pitch angle.

Figure 13. Rotor hover performance (continued).

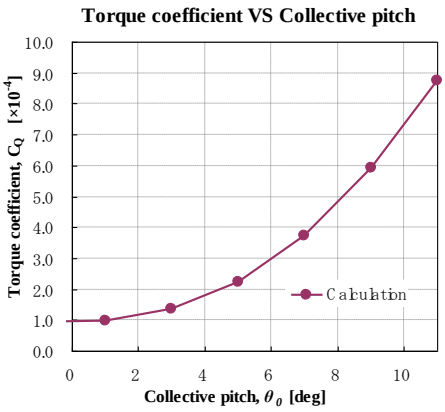

(b) Torque coefficient vs pitch angle.

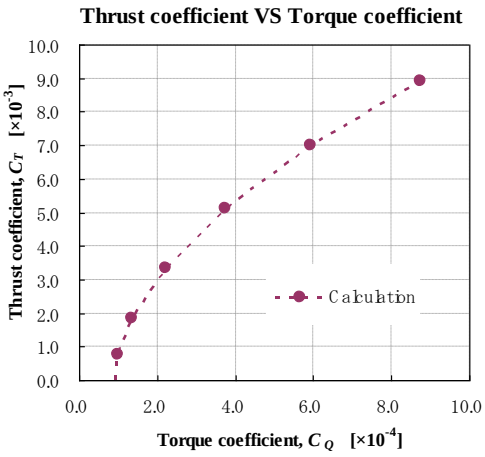

(c) Polar curve

Figure 13. Rotor hover performance (concluded).

Figure 14 shows the surface pressure distribution of NINJA blade in hover. The calculation conditions are as follows: rotor tip speed is 200 m/s and blade pitch angle at root position are shown in the figures. Active flap is not employed in this calculation.

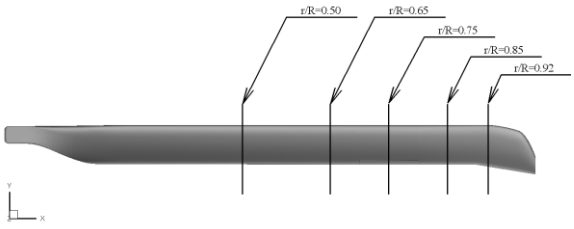

(a) Blade sectional position for comparison

Figure 14. Surface pressure distribution at each spanwise position in hover (continued).

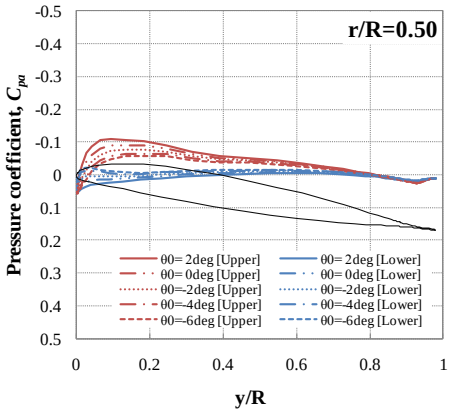

(b) r/R=0.5

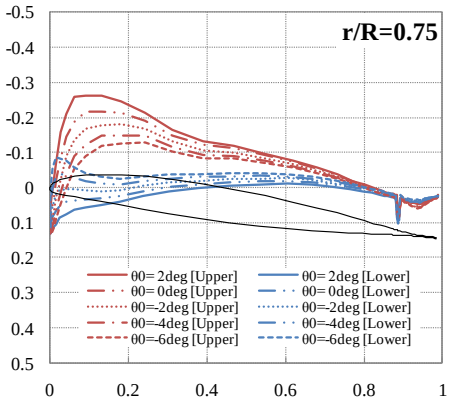

(c) r/R=0.75

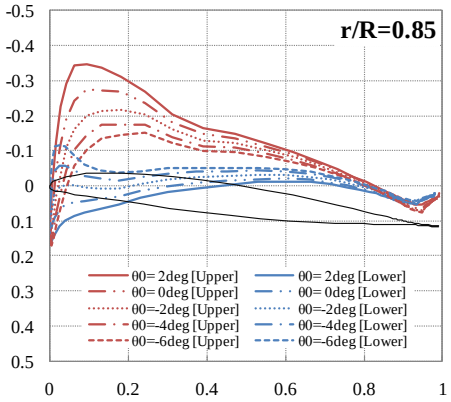

(d) r/R=0.85

Figure 14. Surface pressure distribution at each spanwise position in hover (concluded).

In figure 15, the vortex system around a NINJA rotor calculated by rFlow3D is shown. In this CFD calculation, a modified SLAU scheme (refs. 31-32) is embedded to handle the all-speed of a flow around the rotor. In this figure, the vortices from the root region of the rotor are well captured. Tip vortices from the tip region are also well maintained under the rotor for one revolution. Though a coarse grid is used in this calculation, rFlow3D code shows the vortex capturing capability.

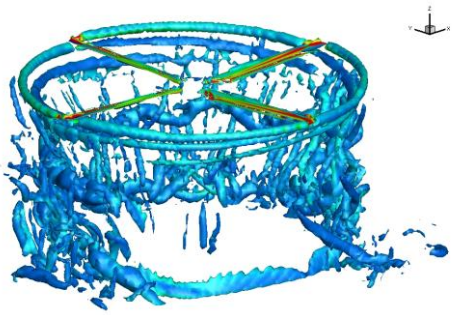

(a) Q-criterion

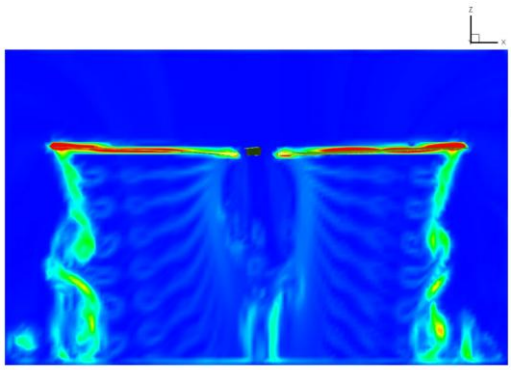

(b) Vortex property at vertical cross section

Figure 15. Vortex structure of NINJA rotor in hovering flight.

Aeroacoustic Predictions

The noise reduction characteristics of the rotor are presented in fig.16 as a function of active flap frequency and phase, where the active flap amplitude is selected for a blade tip deflection equal to 1.5 deg. The derivation of these noise levels is made by following the means of ICAO regulation. Figure 16 shows the relatively large noise reduction capability for each frequency from 2 to 5/rev if 1.5 deg blade tip deflection is assumed. The flight conditions are taken as velocity of 66 kt and descending angle of 6 deg. Among the active flap frequencies, 2/rev is considered most efficient and preferable because of

low required power for actuation and least adverse effect for rotor vibration generated as by-product.

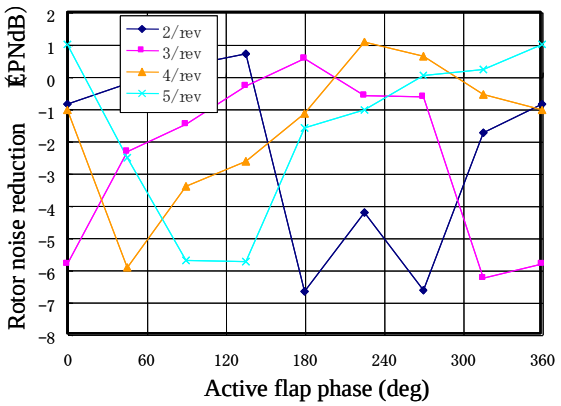

Figure 16. BVI noise reduction characteristics.

CONCLUDING REMARKS

The Novel Intelligent JAXA Active Rotor (NINJA Rotor) program, a cooperative effort between JAXA and NASA, has been described. The preliminary calculation has been conducted. The next steps in the program include more extensive pretest predictions of the expected performance, noise, loads, and vibration; and preparations for the whirl tower test in 2013. The test in the 40- by 80-Foot Wind Tunnel at Ames Research Center is anticipated in 2015.

REFERENCES

1) Shaw, J. “Higher Harmonic Blade Pitch Control: A System for Helicopter Vibration Reduction.” Doctor of Philosophy Thesis, Massachusetts Institute of Technology, 1980.

2) Hassan, A.A.; Charles, B.D.; Tadghighi, H.; and Sankar, L.N. “Blade-Mounted Trailing Edge Flap Control for BVI Noise Reduction.” NASA CR 4426, February 1992.

3) Straub, F.K. “A Feasibility Study of Using Smart Materials for Rotor Control.” Smart Materials and Structures, 5:1 (February 1996).

4) Chopra, I. “Status of Application of Smart Structures Technology to Rotorcraft Systems.” Journal of the American Helicopter Society, 45:4 (October 2000).

5) Dawson, S.; Marcolini, M.; Booth, E.; Straub, F.; Hassan, A.; Tadghighi, H.; and Kelly, H. “Wind Tunnel Test of an Active Flap Rotor: BVI Noise and Vibration Reduction.” American Helicopter Society 51st Annual Forum, Ft. Worth, TX, May 1995.

6) Kobiki, N.; Tsuchihashi, A.; Murashige, A.; and Yamakawa, E. “Elementary Study for the Effect of HHC and Active Flap on Blade Vortex Interaction.” Twenty-Third European Rotorcraft Forum, Dresden, Germany, September 1997.

7) Fulton, M.V., and Ormiston, R.A. “Small-Scale Rotor Experiments with On-Blade Elevons to Reduce Blade Vibratory Loads in Forward Flight.” American Helicopter Society 54th Annual Forum, Washington, D.C., May 1998.

8) Koratkar, N.A., and Chopra, I. “Analysis and Testing of Mach-Scaled Rotor with Trailing-Edge Flaps.” AIAA Journal, 38:7 (July 2000).

9) Enenkl, B.; Kloppel, V.; and Preissler, D. “Full Scale Rotor With Piezoelectric Actuated Blade Flaps.” Twenty-Eighth European Rotorcraft Forum, Bristol, United Kingdom, September 2002.

10) Kobiki, N.; Kondo, N.; Saito, S.; Akasaka, T.; and Tanabe, Y. “An Experimental Study of On-Blade Active Tab for Helicopter Noise Reduction.” Thirtieth European Rotorcraft Forum, Marseilles, France, September 2004.

11) Kobiki, N.; Saito, S.; Akasaka, T.; Tanabe, Y.; and Fuse, H. “An Experimental Study for Aerodynamic and Acoustic Effects of On-Blade Active Tab.” Thirty-First European Rotorcraft Forum, Florence, Italy, September 2005.

12) Delrieux, Y.; Le Pape, A.; Leconte, P.; Crozier, P.; Gimonet, B.; and des Rochettes, H.M. “Wind-Tunnel Assessment of the Concept of Active Flaps on a Helicopter Rotor Model.” American Helicopter Society 63th Annual Forum, Virginia Beach, VA, May 2007.

13) Roget, B., and Chopra, I. “Wind-Tunnel Testing of Rotor with Individually Controlled Trailing-Edge Flaps for Vibration Reduction.” Journal of Aircraft, 45:3 (May-June 2008).

14) Straub, F.K. “Active Flap Control for Vibration Reduction and Performance Improvement.” American Helicopter Society 51st Annual Forum, Ft. Worth, TX, May 1995.

15) Straub, F.K., and Kennedy, D.K. “Design, Development, Fabrication and Testing of an Active Flap Rotor System.” American Helicopter Society 61st Annual Forum, Grapevine, TX, June 2005.

16) Lorber, P.F.; O’Neill, J.J.; Isabella, B.; Andrews, J.; Wong, J.; Hein, B.; Geiger, D.; Wake, B.E.; Jonsson, U.; Sun, F. “Whirl Test of a Large Scale High Authority Active Flap Rotor.” American Helicopter Society 66th Annual Forum, Phoenix, AZ, May 2010.

17) Wei, F.-S., and Weisbrich, A.L. “Multicyclic Controllable Twist Rotor Data Analysis.” NASA CR 152251, January 1979.

18) Straub, F.K.; Anand, V.R.; Birchette, T.S.; and Lau, B.H. “Wind Tunnel Test of the SMART Active Flap Rotor.” American Helicopter Society 65th Annual Forum, Grapevine, TX, May 2009.

19) JanakiRam, R.D.; Sim, B.W.; Kitaplioglu, C.; and Straub, F.K. “Blade-Vortex Interaction Noise Characteristics of a Full-Scale Active Flap Rotor.” American Helicopter Society 65th Annual Forum, Grapevine, TX, May 2009.

20) Hall, S.R.; Anand, V.R.; Straub, F.K.; and Lau, B.H. “Active Flap Control of the SMART Rotor for Vibration Reduction.” American Helicopter Society 65th Annual Forum, Grapevine, TX, May 2009.

21) Roth, D.; Enenkl, B.; and Dieterich, O. “Active Rotor Control by Flaps for Vibration Reduction - Full Scale Demonstrator and First Flight Test Results.” Thirty-Second European Rotorcraft Forum, Maastricht, The Netherlands, September 2006.

22) Dieterich, O.; Enenkl, B.; and Roth, D. “Trailing Edge Flaps for Active Rotor Control. Aeroelastic Characteristics of the ADASYS Rotor System.” American Helicopter Society 62th Annual Forum, Phoenix, AZ, May 2006.

23) Aoyama, T.; Yang, C.; and Saito, S. “Numerical Analysis of Active Flap for Noise Reduction Using Moving Overlapped Grid Method.” Journal of the American Helicopter Society, 52:3 (July 2007).

24) Yang, C.; Aoyama, T.; and Saito, S. “Numerical Analysis of BVI Noise Reduction Using Active Flap Control.” Thirty-First European Rotorcraft Forum, Florence, Italy, September 2005.

25) Bain, J.; Potsdam, M.; Sankar, L.; and Brentner, K.S. “Aeromechanic and Aeroacoustic Predictions of the Boeing SMART Rotor Using Coupled CFD/CSD Analysis.” American Helicopter Society 66th Annual Forum, Phoenix, AZ, May 2010.

26) Ananthan, S.; Baeder, J.; Sim, B. W.-C.; Hahn, S.; and Iaccarino, G. “Prediction and Validation of the Aerodynamics, Structural Dynamics, and Acoustics of the SMART Rotor Using a Loosely-Coupled CFD-CSD Analysis.” American Helicopter Society 66th Annual Forum, Phoenix, AZ, May 2010.

27) Potsdam, M.; Fulton, M.V.; and Dimanlig, A. “Multidisciplinary CFD/CSD Analysis Of The Smart Active Flap Rotor.” American Helicopter Society 66th Annual Forum, Phoenix, AZ, May 2010.

28) Kobiki, N.; Saito, S.; Fukami, T.; and Komura, T. “Design and Performance Evaluation of Full Scale On-Board Active Flap System.” American Helicopter Society 63th Annual Forum, Virginia Beach, VA, May 2007.

29) Kobiki, N., and Saito, S. “Performance Evaluation of Full Scale On-Board Active Flap System in Transonic Wind Tunnel.” American Helicopter Society 64th Annual Forum, Montreal, Canada, April 2008.

30) Johnson, W., “Technology Drivers in the Development of CAMRAD II,” American Helicopter Society Aeromechanics Specialists' Conference, San Francisco, CA, January 19–21, 1994.

31) Tanabe, Y. and Saito, S. “Significance of all-speed Scheme in Application to Rotorcraft CFD Simulations” The 3rd International Basic Research Conference on Rotorcraft Technology” Nanjing, China, October 14-16, 2009.

32) Tanabe, Y. and Saito, S. “Experimental and Numerical Studies of Rotor/Fuselage Interactions” American Helicopter Society Aeromechanics Specialists' Conference, San Francisco, CA, January 19–21, 1994